Atomic structure of an FeCrMoCBY metallic glass revealed by high energy x-ray diffraction

Pussi Katariina, Louzguine-Luzgin Dmitri, Nokelainen Johannes, Barbiellini Bernardo, Kothalawala Veenavee, Ohara Koji, Yamada Hiroki, Bansil Arun, Kamali Saeed

Atomic structure of an FeCrMoCBY metallic glass revealed by high energy x-ray diffraction

K. Pussi[*]

Physics Department, School of Engineering Science, LUT University, 53851 Lappeenranta, Finland and
Natural Resources Institute Finland (Luke), Production Systems, 00790 Helsinki, Finland

D. V. Louzguine-Luzgin

Advanced Institute for Materials Research (WPI-AIMR), Tohoku University, Sendai 980-8577, Japan and
MathAM-OIL, National Institute of Advanced Industrial Science and Technology (AIST), Sendai 980-8577, Japan

J. Nokelaineni and B. Barbiellini

Physics Department, School of Engineering Science, LUT University, 53851 Lappeenranta, Finland and
Physics Department, Northeastern University, Boston, MA 02115, United States

V. Kothalawala

Physics Department, School of Engineering Science, LUT University, 53851 Lappeenranta, Finland

K. Ohara and H. Yamada

Japan Synchrotron Radiation Research Institute, SPring-8,
1-1-1 Kouto, Sayo-cho, Sayo-gun, Hyogo 679-5198 Japan

A. Bansil

Physics Department, Northeastern University, Boston, MA 02115, United States

S. Kamali[†]

Department of Mechanical, Aerospace and Biomedical Engineering,
University of Tennessee Space Institute, Tullahoma, TN 37388 United States and
Department of Physics and Astronomy, Middle Tennessee State University, Murfreesboro, TN 37132, United States
(Dated: May 14, 2022)

Amorphous bulk metallic glasses with the composition $Fe_{48}Cr_{15}Mo_{14}C_{15}B_6Y_2$ have been of interest due to their special mechanical and electronic properties, including corrosion resistance, high yield-strength, large elasticity, catalytic performance, and soft ferromagnetism. Here, we apply a reverse Monte Carlo technique to unravel the atomic structure of these glasses. The pair-distribution functions for various atomic pairs are computed based on the high-energy x-ray diffraction data we have taken from an amorphous sample. Monte Carlo cycles are used to move the atomic positions until the model reproduces the experimental pair-distribution function. The resulting fitted model is consistent with our *ab-initio* simulations of the metallic glass. Our study contributes to the understanding of functional properties of Fe-based bulk metallic glasses driven by disorder effects.

I. INTRODUCTION

Fe-based Fe-Cr-Mo-C-B-Y Bulk Metallic Glasses (BMGs) exhibit a homogeneous non-periodic structure on microscopic and macroscopic scales [1–4]. These alloys support compression strengths that are substantially superior to those of their crystalline counterparts [5–10]. Zhang *et al.* [11] have pointed out the promising potential of BMGs in functional and structural applications. Addition of rare-earths (RE) such as Y and refractory metals such as Mo enhance the glass-forming ability of Fe-based BMGs [1, 12–18], while Cr and Mo improve their corrosion resistance [19]. Interestingly, it was observed that glass formation in the $Fe_{48}Cr_{15}Mo_{14}C_{15}B_6Y_2$ alloy is controlled not by the crystal nucleation rate, but by the crystal growth rate [20, 21]. The many interesting physical,

mechanical, and magnetic properties as well as the high thermal stability of the BMGs are reviewed by Suryanarayana and Inoue [22]. Recently, Sun *et al.* [23] have shown that the surface of $Fe_{48}Cr_{15}Mo_{14}C_{15}B_6Y_2$ behaves also as a catalyst for water dissociation and hydrogen evolution processes. These functional properties of materials often arise from competing phases [24], which break symmetries and generally promote disorder and heterogeneity. However, local bonding considerations still provide strong constraints and, as a result, the observed structures tend to contain local orderings and remain far from being completely random. Heterogeneity and disorder are important in connection with functional properties of materials. In CoFeB alloys, for example, disorder helps enhance spin polarization of the material [25].

Here, in considering $Fe_{48}Cr_{15}Mo_{14}C_{15}B_6Y_2$, our focus is on its microscopic structure. Since the atomic structure plays an essential role in understanding the atomic packing of BMGs [26], we compare the experimental Pair Distribution Function (PDF) [27] obtained using High-Energy X-Ray

---

[*] katariina.pussi@lut.fi
[†] skamalim@utk.edu

Diffraction (HE-XRD) with the results of structural models obtained via Monte Carlo methods based on the Metropolis algorithm. Our approach unravels the atomic structure of this complex material in large unit cells and complements results obtained via first-principles Density Functional Theory (DFT) based computations on smaller cells [23]. Our study thus provides a baseline for structural models based on PDF analysis needed to understand the relationship between the atomic and electronic structures of $Fe_{48}Cr_{15}Mo_{14}C_{15}B_6Y_2$.

II. TOTAL SCATTERING AND PDF FUNDAMENTALS

The total structure factor [28, 29], $S(Q)$, is a function of the absolute wave number Q ($Q = |Q| = (4\pi/\lambda)sin\theta$), where λ is the wavelength of the incident x-rays and θ is the scattering angle. $S(Q)$ is related to the coherent part ($I^{coh}(Q)$) of the diffraction data [30] as follows:

$$S(Q) = 1 + \frac{I^{coh}(Q) - \Sigma C_i |f_i(Q)|^2}{|\Sigma C_i f_i(Q)|^2} , \quad (1)$$

where $f_i(Q)$ is the atomic scattering factor and C_i is the atomic concentration of atomic species of type i. The reduced PDF, $G(r)$, is given by the Fourier transform of $Q[S(Q)-1]$:

$$G(r) = \frac{2}{\pi} \int_{Q_{min}}^{Q_{max}} Q[S(Q) - 1] \sin(Qr) dQ , \quad (2)$$

and it can be expressed as:

$$G(r) = 4\pi r[(\rho(r) - \rho_0)] , \quad (3)$$

where ρ_0 is the atomic number density of the material and $\rho(r) = \rho_0 g(r)$ is the atomic pair density proportional to the PDF denoted by $g(r)$. The peaks of $G(r)$ and $g(r)$ are associated with atomic distances. In order to improve spatial resolution of $G(r)$, $S(Q)$ must be measured with a higher Q cut-off Q_{max}, which becomes possible with the high photon energies available in HE-XRD experiments. The radial distribution function (RDF) is obtained from $g(r)$ as [31]:

$$RDF(r) = 4\pi r^2 \rho_0 g(r) . \quad (4)$$

The PDF approach has been shown to be a useful method for determining structures of non-crystalline and disordered materials as well as nanoparticles [25, 30, 32–53].

III. EXPERIMENTAL DETAILS

The $Fe_{48}Cr_{15}Mo_{14}C_{15}B_6Y_2$ ingot was prepared by arc-melting mixtures of pure metals (99.9 mass% purity), graphite C (99.95 mass% purity), and B (99.99 mass% purity) under an argon atmosphere. From this ingot, ribbon samples of about 20 μm thickness and 1 mm width were prepared by melt spinning onto a single copper roller at a roller tangential velocity of about 40 m/s. By using Mössbauer spectroscopy, we checked that there was no detectable signal from iron-oxide
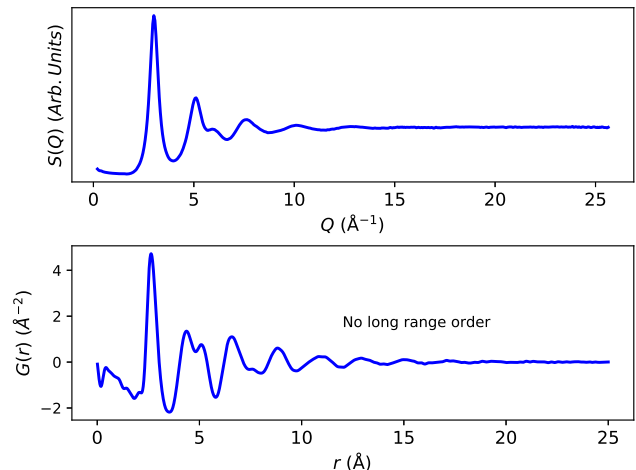

FIG. 1. Upper panel: Experimental S(Q) data. Lower panel: G(r) data calculated from the S(Q) data. G(r) starts to decay after 10 Å, which indicates that there is no long-range order in our sample. Splitting of the second peak in G(r) is an indication of random icosahedral packing in the structure [56]

to rule out the presence of oxygen in our sample. Notably, if a high amount of oxygen is dissolved in a liquid, it would hard for the sample to be vitrified.

HE-XRD measurements were performed with a photon wavelength of 0.21 Å in the transmission mode at beamline BL04B2 of the Japanese synchrotron facility SPring-8. An ionization chamber was used for monitoring the intensity of incident x-rays, while four CdTe and three Ge detectors were used for monitoring the intensity of the scattered x-rays. Furthermore, a two-axis diffractometer installed at BL04B2 was used to cover low Q (small angle) region (≈ 0.1 Å^{-1}). The setup for HE-XRD at this beamline is described in more detail elsewhere [54, 55]. To achieve a high real-space resolution, the full 2θ range for the analysis was used to obtain the structure factor up to 25.6 Å^{-1}.

IV. REVERSE MONTE CARLO METHOD

For amorphous materials, the refinement of structural models is not straightforward due to the large number of atoms that need to be included in the model structures. The Reverse Monte Carlo (RMC) method [57] allows the determination of the atomic structures, which are derived directly from the experimental data. It involves searching for an atomic configuration that can reproduce the $G(r)$ of the unknown structure within a designated χ^2 tolerance. The RMC-generated configuration is thus a viable candidate for the structure of the target [58]. To limit the number of candidate structures, one can add additional constraints involving restraints-based bond lengths.

The experimental PDF was analyzed using the public domain software RMCProfile [59] (version 6), see website rmcprofile.org for details. The main input is the temperature that

determines the mean-square atomic displacements; for other details concerning the generation of initial structures, we refer to the documentation of RMCProfile. Specifically, we model the structure using a simulation box containing a $50 \times 50 \times 50$ Å^3 cluster with 5440 atoms, which is sufficient for capturing important features of $G(r)$ [60].

We started our optimization process with a random arrangement of atoms in the cluster, which was produced via the program *dwbuild* contained within the RMCProfile package [59]. The cut-off lengths were 2.20, 2.20, 2.30, 1.70, 1.80, 2.80, 2.20, 2.30, 1.70, 1.80, 2.80, 2.40, 1.90, 2.00, 3.00, 1.20, 1.40, 2.30, 1.40, 2.50, and 3.20 Å for Fe-Fe, Fe-Cr, Fe-Mo, Fe-C, Fe-B, Fe-Y, Cr-Cr, Cr-Mo, Cr-C, Cr-B, Cr-Y, Mo-Mo, Mo-C, Mo-B, Mo-Y, C-C, C-B, C-Y, B-B, B-Y, and Y-Y atomic pairs, respectively. Some polyhedral restraints follow from these bond-length restraints and are described in the RMCProfile manual. During the optimization process, atoms were allowed to move and swap within the simulation cube, where the atomic moves were controlled by a Metropolis algorithm. [These moves are restricted by the distance-window used.]

V. COMBINING RMC AND DFT

Typically, RMC method gives a snapshot view of about 10^4 atoms. This number of atoms is much larger than that used normally in DFT computations, although system sizes amenable to first-principles treatment have been growing with the increasing availability of high-performance computing resources.[61]. White *et al.* [62] has discussed advantages of combining DFT and PDF analysis. Recent studies [63, 64] have shown that RMC alone is sometimes not sufficient to represent the full picture. RMC in conjunction with first-principles validation, however, can yield improved structures. Accordingly, we have carried out spin-polarized electronic structure calculations using the projected augmented wave (PAW) method implemented in the Vienna Ab-initio Simulation Package (VASP) [65–67]. The Generalized Gradient Approximation (GGA) parameterized by Perdew, Burke, and Ernzerhof [68] was used to account for exchange-correlation effects. Effects of gradient corrections, which are included in the GGA, are important for capturing magnetic properties of Fe [69]. A plane wave cut-off energy of 500 eV was used. The k-points within the Brillouin zone were generated using a uniform $2 \times 2 \times 2$ Monkhorst-Pack [70] mesh. A relatively small subset of our larger atomic cluster that is representative of the stoichiometry of the actual material was selected to execute DFT calculations. The atomic structure was next relaxed, starting with coarse settings, followed by increasing the precision and adding magnetism with randomized initial magnetic moments. Total electronic energy was minimized with a tolerance of 10^{-4} eV. The conjugate-gradient algorithm was used to relax atomic structures until all residual forces converged to within 0.1 eV/Å. A Gaussian-smearing width of 0.05 eV (full-width-at-half-maximum) was applied to the electronic states. Similar calculations have been reported by Sun *et al.* [23], Yu *et al.* [26], and Kazimorov [71]. Our largest model used to carry out DFT computations to sim-

ulate $G(r)$ contained 212 atoms with an average density of 7.8 g/cm^3 after relaxation, which is consistent with the corresponding experimental values [20]. The selfconsistently determined magnetic moments on the iron atoms are random, and range from 0-1.45 μ_B, with most of them being less than 1 μ_B.

VI. RESULTS AND DISCUSSION

The experimental $S(Q)$ and $G(r)$ data are shown in Figure 1, which illustrates the decay of the oscillating features over wide momentum and position ranges. Our $G(r)$ results agree well with those of Liang *et al* [60] based on the HE-XRD experiments at lower 60 keV x-ray energy. In the lower panel of Figure 1, $G(r)$ shows strong oscillations over 2 to about 10 Å. It reflects the presence of well-defined short-range order as well as signatures of amorphous traits [72]. Splitting of the second peak in Fig. 2 has been explained by Clarke and Jonson [56] to be a result of packing of spherical particles, where linear trimers of spheres are responsible for the second subpeak and the first subpeak arises partly from the face-sharing tetrahedra. Figure 5 of Ref. 56 illustrates the three basic atomic configurations that give rise to dominant contributions to the second peak in $G(r)$; these authors also show that the first subpeak grows more than the second subpeak as the random icosahedral packing becomes denser. Pan *et al.* [73] have shown that this splitting does not occur in the liquid phase due to the lower density of the liquid compared to the glass. Preference for icosahedral short-range order derives from the tendency toward efficient atomic packing [74, 75] in metallic glasses.

The PDF fit obtained through RMCProfile is shown in Figure 2. The agreement with experiment is excellent. In particular, the important splitting of the second peak is well reproduced. Selected partial PDFs shown in Figure 3 demonstrate that the first small peak at around 2 Å is mainly from the contribution between the transition metal (Fe/Cr/Mo) and C/B atoms, while the second peak, which is the main peak in $G(r)$, arises mainly from the contribution of transition metals. The wide double peak in the range of 4-6 Å appears from hybridization effects between the various atoms. Our partial PDFs are consistent with those of Kazimorov [71], who discusses how the elastic properties are related to the atomic structural features.

Figure 4 shows the optimized structure of the large cluster corresponding to the fit in Figure 2. For the purpose of visualization, Figure 5 presents a small 76 atom cluster that is cut from the center of our RMC model. 70% of nearest neighbors in this structure are Fe-Fe, Fe-Cr, or Fe-Mo, which thus form the skeleton of the cluster. Second largest group (14%) of nearest neighbors are Cr-Cr, Cr-Mo, and Mo-Mo. RMC finds that the most populous coordination number is 6 and that the average coordination is 5.65.

Our DFT-based $G(r)$ is compared with the corresponding experimental results in Figure 6. A good overall agreement is seen despite a relatively small number of atoms in the DFT simulation. Our RMC model is also used as input of *ab-initio*
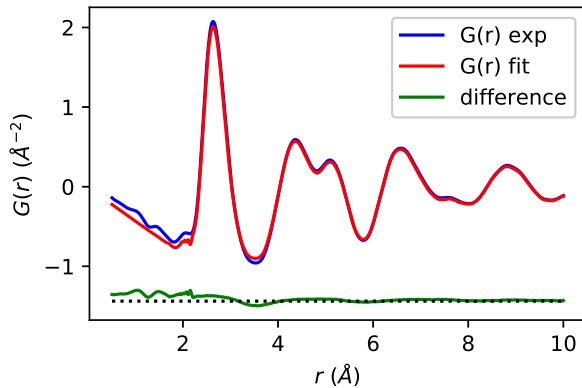
FIG. 2. Comparison of the experimental and RMC model $G(r)$. The experimental data are rescaled by the factor of 0.4395.
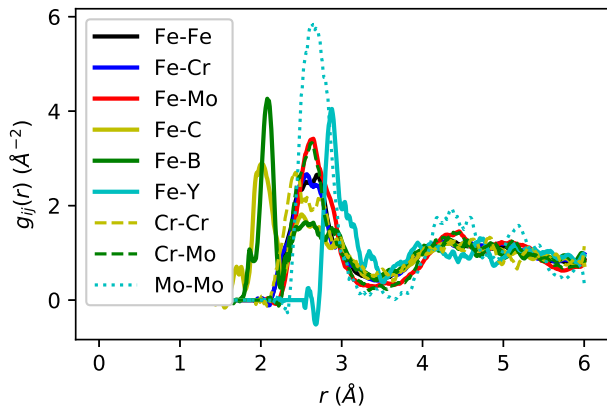

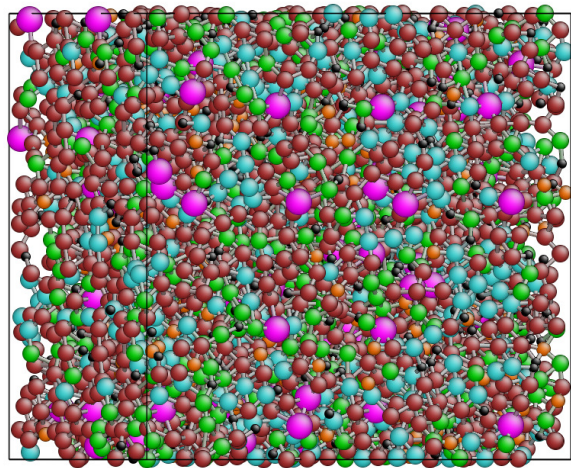FIG. 3. Partial PDFs for selected atomic pairs.

FIG. 4. Optimized structure. The average coordination is 5.6 (most populous = 6). Color coding is as follows. Brown = Fe, Green = Cr, cyan = Mo, Black = C, Orange = B, Magenta = Y.

MD simulations of the metallic glass performed on small periodic clusters, while providing non-periodic information on larger unit cells involving about 5440 atoms, which are useful for visualizing the nanoscale spatial heterogeneity of metallic glasses [76]. The $G(r)$ in Figure 6 varies linear in the low-r region with a slope of $-4\pi\rho_0$, where ρ_0 is the average density, see Peterson *et al.* [77]. This slope is very well described by our DFT model.

VII.   CONCLUSIONS

We have presented an inverse method in which total x-ray scattering is used to determine the structure of Fe-based bulk metallic glasses. The method yields an RMC structural model with a cluster of 5440 atoms in excellent agreement with the corresponding experimental data. This fitted model is consistent with our DFT-based simulations using a periodic cell containing 212 Fe atoms. Our atomic structure reveals the presence of spatial heterogeneity [76] in the glass with nanoscale density fluctuations. The densely packed regions host an icosahedral order [75] reflected in the splitting of the second $G(r)$ peak [56], while less dense regions exhibit tetrag-
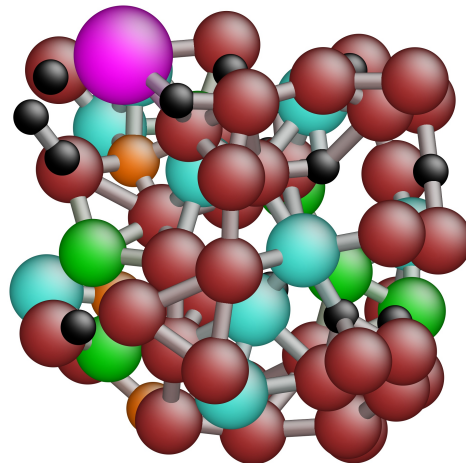

FIG. 5. 76-atom cluster cut from the center of our RMC computational cube. Color coding is as follows. Brown = Fe, Green = Cr, cyan = Mo, Black = C, Orange = B, Magenta = Y.

onal order linked to the formation of covalent bonds. Zhou *et al.* [76] have characterized this type of heterogeneity by utilizing state-of-the-art angstrom-beam electron diffraction and scanning-transmission electron microscopy to explain why the amplitude-modulation dynamic atomic-force microscopy cannot probe the nature of nanoscale domains. Magnetic force microscopy could provide a better window on the spatial heterogeneity [79]. Our structural model would provide a realistic basis for modeling electronic structures and densities
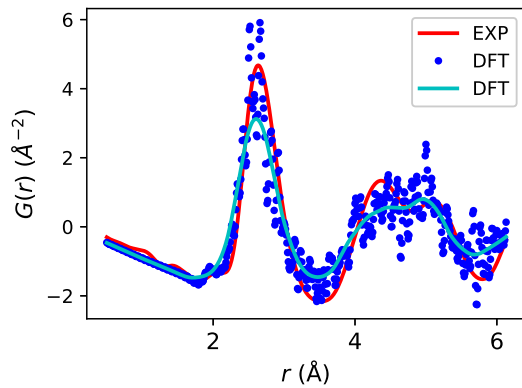
FIG. 6. Comparison of the experimental and DFT-based $G(r)$. The DFT points (blue) have been smoothed with a moving average (green curve) to facilitate comparison with the experimental data (red curve). See Ref. [78] for the smoothing algorithm used.

of states for addressing the unique properties of amorphous

steels, which involve a subtle interplay of metallic and covalent bondings [71].

[1] H. S. Chen, Rep. Prog. Phys. **43**, 353 (1980).
[2] A. L. Greer, Science **267**, 1945 (1995).
[3] A. Inoue, Acta Mater **48**, 279 (2000).
[4] W. L. Johnson, MRS Bull **24**, 42 (1999).
[5] A. Inoue, Y. Shinohara, and J. S. Gook, Mater. Trans. JIM **36**, 1427 (1995).
[6] A. Inoue, A. Takeuchi, and T. Zhang, Metallurgical and Mater. Trans. A **29**, 1779 (1998).
[7] S. J. Pang, T. Zhang, K. Asami, and A. Inoue, Mater. Trans. JIM **42**, 376 (2001).
[8] X. J. Gu, S. J. Poon, G. J. Shiflet, and M. Widom, Acta Mater **56**, 88 (2008).
[9] T. D. Shen and R. B. Schwarz, Acta Mater **49**, 837 (2001).
[10] A. Inoue, B. L. Shen, and C. T. Chang, Acta. Materiala **52**, 4093 (2004).
[11] T. Zhang, F. Liu, S. J. Pang, and R. Li, Mater. Trans. **48**, 1157 (2007).
[12] Z. P. Lu, C. T. Liu, and W. D. Porter, Appl. Phys. Lett. **83**, 2581 (2003).
[13] Z. P. Lu, C. T. Liu, J. R. Thompson, and W. D. Porter, Phys. Rev. Lett. **92**, 245503 (2004).
[14] V. Ponnambalam, S. J. Poon, and G. J. Shiflet, J. Mater. Res. **19**, 1320 (2004).
[15] K. Amiya and A. Inoue, Mater. Trans. **47**, 1615 (2006).
[16] T. A. Baser and M. Baricco, J. of Alloys and Comp. **190**, 14569 (2006).
[17] Q. Chen, D. Zhang, J. Shen, H. Fan, and J. Sun, J. of Alloys Comp. **427**, 190 (2007).
[18] X. Yang, X. Ma, Q. Li, and S. Guo, Journal of Alloys and Compounds **554**, 446 (2013).
[19] M. J. Duarte, J. Klemm, S. O. Klemm, K. J. J. Mayrhofer, M. Stratmann, S. Borodin, A. H. Romero, M. Madinehei, D. Crespo, J. Serrano, S. S. A. Gerstl, P. P. Choi, D. Raabe, and F. U. Renner, Science **341**, 372 (2013).
[20] D. V. Louzguine-Luzgin, A. I. Bazlov, S. V. Ketov, and A. Inoue, Materials Chemistry and Physics **162**, 197 (2015).
[21] D. V. Louzguine-Luzgin, A. I. Bazlov, S. V. Ketov, A. L. Greer, and A. Inoue, Acta Materialia **82**, 396 (2015).
[22] C. Suryanarayana and A. Inoue, International Materials Reviews **58**, 131 (2013).
[23] P.-P. Sun, D. R. Kripalani, and K. Zhou, Phys. Chem. Chem. Phys. **22**, 700 (2020).
[24] T. Lookman and P. Littlewood, MRS bulletin **34**, 822 (2009).
[25] K. Pussi, B. Barbiellini, K. Ohara, H. Yamada, J. Dwivedi, A. Bansil, A. Gupta, and S. Kamali, Journal of Physics: Condensed Matter **33**, 395801 (2021).
[26] Q. Yu, X. Wang, H. Lou, Q. Cao, and J. Jiang, Acta Materialia **102**, 116 (2016).
[27] S. J. Billinge, Philosophical Transactions of the Royal Society A **377**, 20180413 (2019).
[28] J.-P. Hansen and I. R. McDonald, *Theory of simple liquids: with applications to soft matter* (Academic press, 2013).
[29] T. E. Faber and J. M. Ziman, The Philosophical Magazine: A Journal of Theoretical Experimental and Applied Physics **11**, 153 (1965).
[30] M. Harada, R. Ikegami, L. S. R. Kumara, S. Kohara, and O. Sakata, RSC Adv. **9**, 29511 (2019).
[31] A. Guinier, Physics Today **22**, 25 (1969).
[32] B. Warren, *x-ray diffraction* (Dover publications, Inc., New York, USA, 1969).
[33] T. Egami and S. Billinge, *Underneath the Bragg Peaks: Structural Analysis of Complex Materials* (Pergamon Press, Oxford, UK, 2003).
[34] S. J. L. Billinge and I. Levin, Science **316**, 561 (2007).
[35] S. K. Pradhan, Z. T. Deng, F. Tang, C. Wang, Y. Ren, P. Moeck, and V. Petkov, J. Appl. Phys. **102**, 044304 (2007).
[36] M. Fernández-García, C. Belver, J. C. Hanson, X. Wang, and J. A. Rodriguez, J. Am. Chem. Soc. **129**, 13604 (2007).
[37] V. Petkov, Materials Today **11**, 28 (2008).
[38] E. S. Bŏzin, C. D. Malliakas, P. Souvatzis, T. Profferì, N. A. Spaldin, M. G. Kanatzidis, and S. . L. Billinge, Science **330**, 1660–1663 (2010).

[39] K. M. Ø. Jensen, E. S. Bŏzin, C. D. Malliakas, M. B. Stone, M. D. Lumsden, M. G. Kanatzidis, S. M. Shapiro, and S. J. L. Billinge, Pysical Review **B86**, 085313 (2012).

[40] D. A. Keen and A. L. Goodwin, Nature **521**, 303 (2015).

[41] F. L. Deepak, M. Bañobre-López, E. Carbó-Argibay, M. F. Cerqueira, Y. Piñeiro-Redondo, J. Rivas, C. M. Thompson, S. Kamali, C. Rodríguez-Abreu, K. Kovnir, and Y. V. Kolen'ko, The Journal of Physical Chemistry C **119**, 11947 (2015).

[42] A. Mancini and L. Malavasi, Chem.Commun. **51**, 16592 (2015).

[43] K. M. Ø. Jensen, A. B. Blichfeld, S. R. Bauers, S. R. Wood, E. Dooryhee, D. C. Johnson, B. B. Iversen, and S. J. L. Billinge, IUCrJ **2**, 481–489 (2015).

[44] K. M. Jensen, P. Juhas, M. A. Tofanelli, C. L. Heinecke, G. Vaughan, C. J. Ackerson, and S. J. Billinge, Nature Communications **7**, 11859 (2016).

[45] A.-C. Dippel, K. M. Ø. Jensen, C. Tyrsted, M. Bremholm, E. D. Bøjesen, D. Saha, S. Birgisson, M. Christensen, S. J. L. Billinge, and B. B. Iversen, ActaCryst. **A72**, 645–650 (2016).

[46] A.-C. Dippel, M. Roelsgaard, U. Boettger, T. Schneller, O. Gutowski, and U. Ruett, IUCrJ **6**, 290–298 (2019).

[47] M. K. Mathiesen, R. Väli, M. Härmas, E. Lust, J. F. Bulow, K. M. Ø. Jensen, and P. Norby, J. Mater. Chem. A **7**, 11709 (2019).

[48] T. L. Christiansen, E. D. Bøjesen, M. Juelsholt, J. Etheridge, and K. M. Ø. Jensen, ACSNano **13**, 8725 (2019).

[49] S. Banerjee, C.-H. Liu, K. M. Ø. Jensen, P. Juhas, J. D.Lee, M. Tofanelli, C. J. Ackerson, C. B. Murray, and S. J. L. Billinge, Acta Cryst. **A76**, 24 (2020).

[50] T. L. Christiansen, S. R. Cooper, and K. M. Ø. Jensen, Nanoscale Adv. **2**, 2234 (2020).

[51] K. Pussi, J. Gallo, K. Ohara, E. Carb-Argibay, Y. V. Koleńko, B. Barbiellini, A. Bansil, and S. Kamali, Condens. Matter **5(1)**, 19 (2020).

[52] K. Pussi, B. Barbiellini, K. Ohara, E. Carbo-Argibay, Y. V. Kolen'ko, A. Bansil, and S. Kamali, Journal of Physics: Condensed Matter **32**, 485401 (2020).

[53] K. Pussi, B. Barbiellini, K. Ohara, H. Yamada, E. Carbo-Argibay, V. Sousa, Y. Kolen'ko, A. Bansil, and S. Kamali, physica status solidi (b) (2022).

[54] S. Kohara, M. Itou, K. Suzuya, Y. Inamura, Y. Sakurai, Y. Ohishi, and M. Takata, Journal of Physics: Condensed Matter **19**, 506101 (2007).

[55] K. Ohara, Y. Onodera, M. Murakami, and S. Kohara, Journal of Physics: Condensed Matter **33**, 383001 (2021).

[56] A. S. Clarke and H. Jónsson, Physical Review E **47**, 3975 (1993).

[57] R. Mcgreevy, Journal of Physics: Condensed Matter **13** (2001).

[58] Y. Cheng and E. Ma, Progress in materials science **56**, 379 (2011).

[59] M. G. Tucker, D. A. Keen, M. T. Dove, A. L. Goodwin, and Q. Hui, Journal of Physics: Condensed Matter **19**, 335218 (2007).

[60] D. Liang, J.-C. Tseng, X. Liu, Y. Cai, G. Xu, and J. Shen, Materials **14** (2021).

[61] A. Erba, J. Baima, I. Bush, R. Orlando, and R. Dovesi, Journal of Chemical Theory and Computation **13**, 5019 (2017), pMID: 28873313.

[62] C. E. White, J. L. Provis, T. Proffen, D. P. Riley, and J. S. J. van Deventer, Phys. Chem. Chem. Phys. **12**, 3239 (2010).

[63] B. Bhattarai, R. Thapa, and D. A. Drabold, Modelling and Simulation in Materials Science and Engineering **27**, 075002 (2019).

[64] A. Pandey, P. Biswas, and D. A. Drabold, Scientific Reports **6**, 1 (2016).

[65] G. Kresse and J. Furthmüller, Phys. Rev. B **54**, 11169 (1996).

[66] G. Kresse and D. Joubert, Phys. Rev. B **59**, 1758 (1999).

[67] G. Kresse and J. Furthmüller, Computational Materials Science **6**, 15 (1996).

[68] J. P. Perdew, K. Burke, and M. Ernzerhof, Phys. Rev. Lett. **77**, 3865 (1996).

[69] B. Barbiellini, E. G. Moroni, and T. Jarlborg, J. Phys. Condens. Matter **2**, 7597 (1990).

[70] H. J. Monkhorst and J. D. Pack, Phys. Rev. B **13**, 5188 (1976).

[71] V. Y. Kazimirov, Phys. Rev. B **80**, 214117 (2009).

[72] Z. H. Stachurski, Materials (Basel, Switzerland) **4**, 1564 (2011).

[73] S. Pan, J. Qin, W. Wang, and T. Gu, Physical Review B **84**, 092201 (2011).

[74] H. Sheng, W. Luo, F. Alamgir, J. Bai, and E. Ma, Nature **439**, 419 (2006).

[75] D. B. Miracle, T. Egami, K. M. Flores, and K. F. Kelton, Mrs bulletin **32**, 629 (2007).

[76] F. Zhu, A. Hirata, P. Liu, S. Song, Y. Tian, J. Han, T. Fujita, and M. Chen, Physical review letters **119**, 215501 (2017).

[77] P. F. Peterson, D. Olds, M. T. McDonnell, and K. Page, Journal of applied crystallography **54**, 317 (2021).

[78] W. S. Cleveland, Journal of the American statistical association **74**, 829 (1979).

[79] P. Geydt, I. D. Rodionov, A. B. Granovsky, E. Soboleva, E. Fadeev, I. S. Titov, I. Dubenko, and E. Lähderanta, in *EPJ Web of Conferences*, Vol. 185 (EDP Sciences, 2018) p. 05004.